

# Probing intermolecular couplings in liquid water with two-dimensional infrared photon echo spectroscopy

A. Paarmann,<sup>1</sup> T. Hayashi,<sup>2</sup> S. Mukamel,<sup>2</sup> and R. J. D. Miller<sup>1,a)</sup>

<sup>1</sup>*Institute for Optical Sciences and Departments of Physics and Chemistry, University of Toronto, Toronto, Ontario M5S 3H6, Canada*

<sup>2</sup>*Department of Chemistry, University of California, Irvine, California 92697-2025, USA*

(Received 10 March 2008; accepted 11 April 2008; published online 19 May 2008)

Two-dimensional infrared photon echo and pump probe studies of the OH stretch vibration provide a sensitive probe of the correlations and couplings in the hydrogen bond network of liquid water. The nonlinear response is simulated using numerical integration of the Schrödinger equation with a Hamiltonian constructed to explicitly treat intermolecular coupling and nonadiabatic effects in the highly disordered singly and doubly excited vibrational exciton manifolds. The simulated two-dimensional spectra are in close agreement with our recent experimental results. The high sensitivity of the OH stretch vibration to the bath dynamics is found to arise from intramolecular mixing between states in the two-dimensional anharmonic OH stretch potential. Surprisingly small intermolecular couplings reproduce the experimentally observed intermolecular energy transfer times. © 2008 American Institute of Physics. [DOI: 10.1063/1.2919050]

## I. INTRODUCTION

The special properties of liquid water ultimately originate from the correlations and intermolecular couplings in the extended hydrogen bond network. The fluctuating local electric fields and the variations in number, strength, and orientation of hydrogen bonds strongly deform the potential energy surfaces. Two-dimensional infrared photon echo (2DIR-PE) spectroscopy has been recently proven to be a very powerful tool for investigating the dynamics of local structures in water.<sup>1–4</sup> Changes in the local environments are directly reflected in modulations of the transition frequencies, dipole moments, and anharmonicities of the stretching vibrations, making the OH stretch mode the most direct probe of structural correlations and fluctuations in the liquid.

Most previous studies have focused on isotopically substituted systems HOD/D<sub>2</sub>O and HOD/H<sub>2</sub>O,<sup>3–6</sup> where the vibrational mode probed is localized on one bond of the molecule and no resonant vibrational energy transfer is observed due to a large separation of the chromophores. Most recently, the first experimental studies on pure H<sub>2</sub>O have shown significantly faster structural dynamics<sup>1,2</sup> compared to the HOD systems. A stronger coupling to librational motions was found to be the main reason for this behavior, although some contributions from resonant energy transfer (ET) and delocalization of the vibrational excitations are also expected.

Explicit treatment of intermolecular vibrational coupling in simulations of the nonlinear vibrational response of water has not yet been demonstrated. Molecular dynamics (MD) based calculations of localized stretching frequency trajectories and subsequent calculation of the nonlinear response without considering intermolecular coupling have been shown;<sup>4,7</sup> fluctuations of the transition dipole moments through non-Condon effects have also been included.<sup>5</sup> Alter-

natively, intermolecular ET was studied by using harmonic approximations.<sup>8,9</sup> In this work, we use numerical integration of the Schrödinger equation<sup>10</sup> (NISE) in a fully anharmonic nonadiabatic simulation procedure, explicitly treating the intermolecular coupling, as well as fluctuations and anharmonicities of transition frequencies and dipole moments, to calculate the 2DIR-PE and pump probe (PP) response of OH stretch vibrations in liquid water. With this new procedure, we find excellent agreement with the recent experimental results.<sup>2</sup>

## II. METHODS

A constant volume simple point charge/extended water MD trajectory of  $N=64$  molecules with 0.5 fs time steps at room temperature was generated using the GROMACS-3.3.1 program.<sup>11</sup> Transition frequencies and dipole moments between six vibrational eigenstates of the OH stretch potential were calculated at each time step and for each molecule using the *ab initio* electrostatic map for the OH stretch vibrations in H<sub>2</sub>O, which is equivalent to the previous work on HOD in D<sub>2</sub>O.<sup>6</sup> The electrostatic potential in the vicinity of a single H<sub>2</sub>O molecule generated by the surrounding molecules is expanded to the second order in Cartesian coordinates. The anharmonic vibrational potential surface of H<sub>2</sub>O in the multipole electrostatic field was expanded in the three normal coordinates in the gas phase. Vibrational transition frequencies between ground state and the five eigenstates (symmetric and antisymmetric O–H stretch, their overtones, and combination) and the transition dipole moments between these states were parametrized with the electrostatic coefficients.<sup>12</sup> To compensate for insufficient solvent shifts produced by the *ab initio* map, we scaled all electric fields with a factor of 2.2 to match the maximum of the fundamental frequency distribution to the maximum of the linear spectrum of H<sub>2</sub>O, as shown in Fig. 1.

<sup>a)</sup>Electronic mail: dmiller@lphys.chem.utoronto.ca.

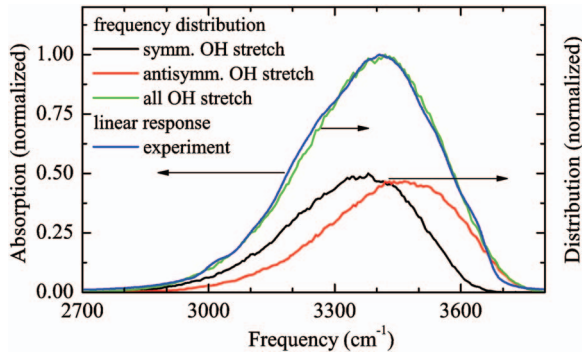


FIG. 1. (Color) Fundamental frequency distribution of the symmetric (black), antisymmetric (red) OH stretch vibration, and combined symmetric and antisymmetric frequency distribution (green). Blue: Experimental linear spectrum (Ref. 13).

We employed the following time dependent effective Hamiltonian for  $M=128$  coupled modes (64 molecules, two modes each), using the anharmonic local eigenstates provided by the electrostatic map as a basis ( $\hbar=1$ ):

$$\begin{aligned} \hat{H}(\tau) = & \sum_m \omega_m(\tau) \hat{B}_m^\dagger \hat{B}_m + \sum_{m' \neq m} J_{m,m'}(\tau) \hat{B}_m^\dagger \hat{B}_{m'} \\ & + \sum_{mn,m'n'} V_{mn,m'n'}(\tau) \hat{B}_m^\dagger \hat{B}_n^\dagger \hat{B}_{m'} \hat{B}_{n'} - \int d\mathbf{r} \hat{\mathbf{P}}(\mathbf{r}) \cdot \mathbf{E}(\mathbf{r}, \tau). \end{aligned} \quad (1)$$

The first two terms describe the free boson system, where  $\omega_m(\tau)$  is the fundamental transition frequency of mode  $m$ ,  $\hat{B}_m^\dagger$  ( $\hat{B}_m$ ) is the boson creation (annihilation) operator for mode  $m$ . The intermolecular coupling  $J_{m,m'}$ , for  $m, m'$  on different molecules, was calculated using resonant dipole-dipole coupling. Since the electrostatic map provides the instantaneous local eigenstates, we set all intramolecular couplings to 0. The last term describes the interaction with the optical fields. The third term contains both intramolecular and intermolecular anharmonicities, the latter arising from anharmonicities in the transition dipole moments, Eq. (2), affecting the dipole-dipole coupling,

$$\begin{aligned} \hat{\mu}(\tau) = & \sum_m \mu_m(\tau) (\hat{B}_m^\dagger + \hat{B}_m) \\ & + \sum_{mmm'} \Delta\mu_{mmm'}(\tau) (\hat{B}_m^\dagger \hat{B}_{m'} \hat{B}_n + \hat{B}_n^\dagger \hat{B}_m^\dagger \hat{B}_{m'}). \end{aligned} \quad (2)$$

Here,  $\mu_m$  is the fundamental transition dipole moment of mode  $m$  and  $\Delta\mu$  is the anharmonicity of the fundamental to overtone transition dipole moment. In Eq. (2), we neglected intermolecular anharmonicities while fully treating all intramolecular anharmonicities of the transition dipole moments.

Calculation of the 2DIR-PE and PP signal requires summation over the contributions from six Liouville pathways. They are commonly referred to as ground state bleach ( $S_1$  and  $S_4$ ), induced emission from the excited state ( $S_2$  and  $S_5$ ), and excited state absorption ( $S_3$  and  $S_6$ ), for the rephasing ( $S_1, S_2, S_3$ ) and nonrephasing ( $S_4, S_5, S_6$ ) phase matching

conditions.<sup>14</sup> For illustration, the nonlinear response functions for the rephasing pathways are given in Eq. (3).

$$S_1 = -\langle \hat{\mu}^- \hat{G}_1^\dagger(\tau_1, \tau_0) \hat{\mu}^+ \hat{G}_0^\dagger(\tau_3, \tau_1) \hat{\mu}^- \hat{G}_1(\tau_3, \tau_2) \hat{\mu}^+ \rangle,$$

$$S_2 = -\langle \hat{\mu}^- \hat{G}_1^\dagger(\tau_2, \tau_0) \hat{\mu}^+ \hat{G}_0^\dagger(\tau_3, \tau_2) \hat{\mu}^- \hat{G}_1(\tau_3, \tau_1) \hat{\mu}^+ \rangle,$$

$$S_3 = -\langle \hat{\mu}^- \hat{G}_1^\dagger(\tau_3, \tau_0) \hat{\mu}^- \hat{G}_2(\tau_3, \tau_2) \hat{\mu}^+ \hat{G}_1(\tau_2, \tau_1) \hat{\mu}^+ \rangle. \quad (3)$$

Here,  $\hat{\mu}^+$  and  $\hat{\mu}^-$  denote dipole excitation and de-excitation operations, respectively. The propagators  $\hat{G}_0$ ,  $\hat{G}_1$ , and  $\hat{G}_2(\tau_b, \tau_a)$  propagate the ground, singly excited, and doubly excited state, respectively, from  $\tau_a$  to  $\tau_b$ .

The propagation was performed using NISE,<sup>8,10</sup>

$$\hat{G}(\tau_b, \tau_a) = -i\theta(\tau_b - \tau_a) \prod_{p=\tau_a}^{\tau_b - \Delta\tau} \exp(-i\hat{H}(p)\Delta\tau), \quad (4)$$

where  $\theta(\tau)$  is the Heaviside function,  $\Delta\tau=2$  fs. The matrix exponential in Eq. (4) was calculated exactly for the single particle propagations  $\hat{G}_1(\tau_b, \tau_a)$ . This is not possible for propagation of the two particle excitations  $\hat{G}_2(\tau_b, \tau_a)$  in diagrams  $S_3$  and  $S_6$  due to the large size of the symmetrized two-particle basis being  $M(M+1)/2$ . These matrix exponentials were calculated by splitting the two-particle Hamiltonian into harmonic [first two terms in Eq. (1)] and anharmonic [third term in Eq. (1)] parts and employing the split-operator method<sup>15</sup> to calculate the total propagator. The harmonic exponential can be calculated exactly from factorization of the single particle propagators, and the small anharmonic part is calculated by first order Taylor expansion.

The photon echo signal was calculated in the impulsive limit. The 2D spectra were obtained by double Fourier transformation with respect to  $t_1$  and  $t_3$ ,  $t_i = \tau_i - \tau_{i-1}$ . The PP signal was also calculated in the impulsive limit setting  $t_1=0$ . The polarization anisotropy (PA)  $r(t_2)$  was calculated<sup>1,16</sup> from spectrally integrated PP signal with parallel and crossed polarization of the pump and probe pulses.

### III. RESULTS AND DISCUSSION

The main focus of this study is on the effect of intermolecular coupling on the vibrational response when entering the fully resonant coupling regime for pure H<sub>2</sub>O. We used the dielectric constant as a scaling factor in the resonant dipole-dipole coupling to reproduce the PA decay regime of  $\approx 80$  fs observed in H<sub>2</sub>O.<sup>1,2,16</sup> Statistical analysis of the intermolecular coupling for a given value of the dielectric constant allows extraction of the average next neighbor coupling strength  $\kappa = \langle |J_{mm'}| \rangle$  for  $R_{mm'} < 3.2$  Å, where  $R_{mm'}$  is the distance between molecules for the local modes  $m$  and  $m'$ .

In Fig. 2, we show the spectrally integrated PP signal for parallel and crossed polarization of pump and probe pulses (a) and the PA calculated from these signals (b) for three coupling regimes. Also shown is the experimentally observed anisotropy decay in H<sub>2</sub>O.<sup>2</sup>

The PA of the uncoupled system shows a fast initial decay due to strong orientational fluctuations of the transition dipole moments, accounting for  $\approx 1/2$  of the signal decay.

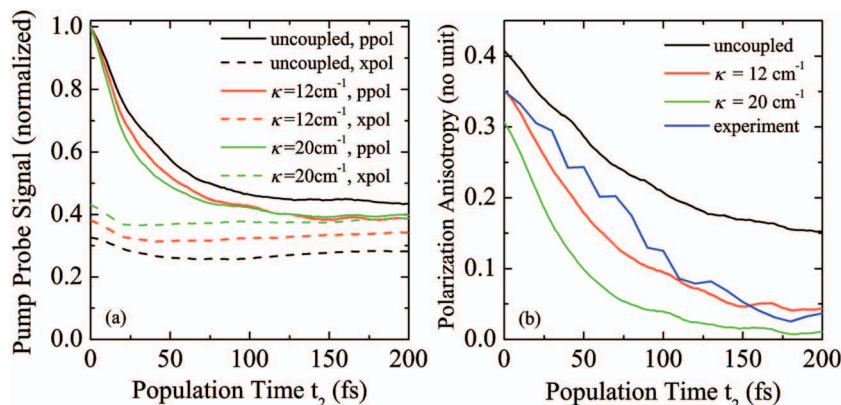


FIG. 2. (Color) Spectrally integrated PP and PA signal. (a) Transients for parallel (ppol) and crossed (xpol) polarization of pump and probe pulses for three coupling regimes. (b) PA calculated from (a). Blue: Experimental PA (Ref. 2).

The remaining contributions are due to librational and slow reorientation dynamics.<sup>12</sup> With increasing coupling strength, the anisotropy decay speeds up and the long-lived components vanish. This effect can clearly be assigned to intermolecular ET which is expected to be at least partially coherent. The anisotropy decay can now be fitted with a single exponential decay, resulting in decay times of 75 fs for  $\kappa=12\text{cm}^{-1}$  and 40 fs for  $\kappa=20\text{cm}^{-1}$ . An additional effect is observed for the initial value of the PA, which is decreasing with increasing coupling strength. Both decay time and initial value of the PA are in excellent agreement with experiment for  $\kappa=12\text{cm}^{-1}$ . Here, we note that the pump probe cross correlation can distort the experimental anisotropy which, however, was found to not affect the observed dynamics within experimental error.

In Fig. 3, we show the 2DIR-PE spectra for two models,  $\kappa=0\text{cm}^{-1}$  (uncoupled) and  $\kappa=12\text{cm}^{-1}$  for population times  $t_2=0, 100, 200, 500$  fs. Two peaks corresponding to the fundamental  $0\rightarrow 1$  transition and excited state  $1\rightarrow 2$  absorption are observed. The  $1\rightarrow 2$  transition is redshifted due to anharmonicities of the vibrational frequencies. A strong interference between these two peaks leading to partial or complete

cancellation of signal in the overlap region, distorts the individual peak shapes, amplitudes, and positions.

In both models at  $t_2=0$  fs, the fundamental peak is stretched along the diagonal, indicating some initial inhomogeneity. As a function of  $t_2$ , the peaks become more vertical on similar time scales for both models, somewhat faster for the  $\kappa=12\text{cm}^{-1}$  system. Due to the interference between the two peaks and the distribution of dynamics across the spectrum, no single time scale for loss of correlations can be extracted from the 2DIR-PE spectra. On closer inspection of the  $\kappa=12\text{cm}^{-1}$  spectra, a bending of the fundamental peak and the nodal lines between the two peaks is observed. This is an indication of faster fluctuations and loss of inhomogeneity on the red side of the spectrum. From our results for  $\kappa=12\text{cm}^{-1}$ , any initial correlations on the red side of the spectrum have decayed by 100 fs, whereas correlations on the blue side persist beyond 200 fs. This finding is in very close agreement with the recent experimental results on the 2DIR-PE spectrum of  $\text{H}_2\text{O}$ .<sup>2</sup>

In Fig. 4, we compare our simulation results for  $\kappa=12\text{cm}^{-1}$  with the experimental spectra.<sup>2</sup> For better com-

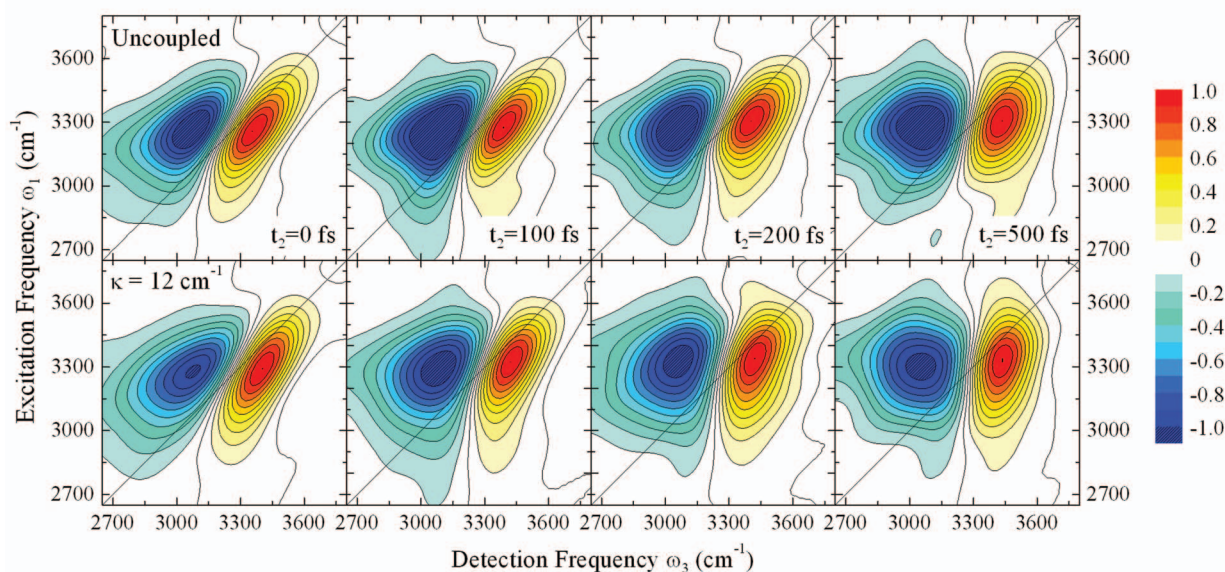


FIG. 3. (Color) 2DIR-PE spectra of the OH stretch vibration in  $\text{H}_2\text{O}$  for population times  $t_2=0, 100, 200, 500$  fs. Top panel: Uncoupled system, bottom panel:  $\kappa=12\text{cm}^{-1}$ . Each spectrum is normalized to its maximum.

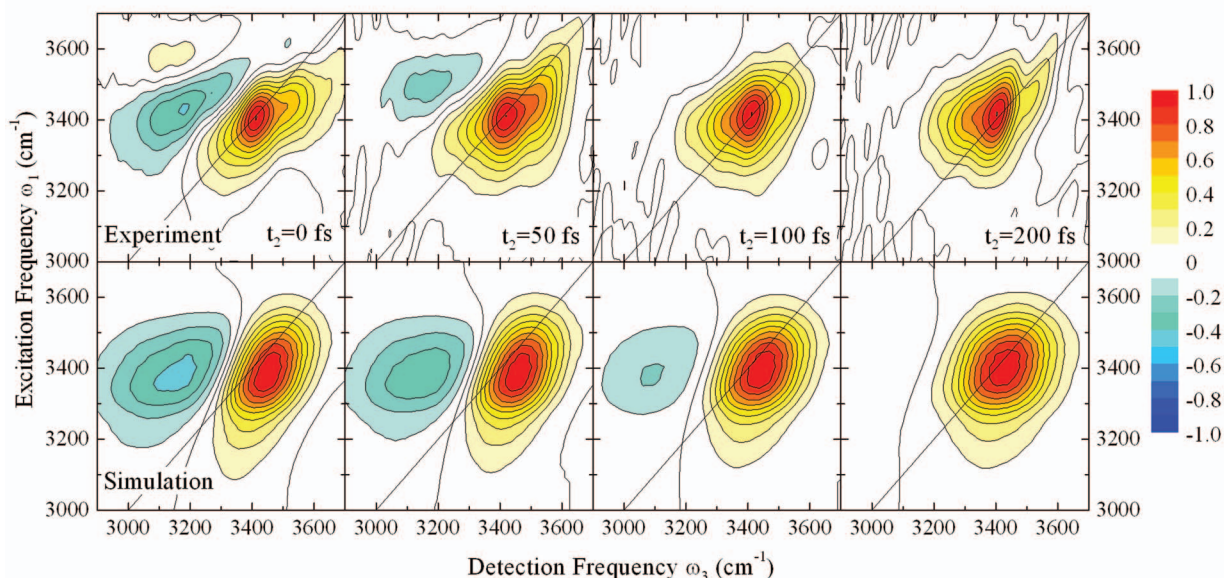


FIG. 4. (Color) 2DIR-PE spectra of the OH stretch vibration in H<sub>2</sub>O for population times  $t_2=0, 50, 100, 200$  fs. Top panel: Experimental data (Ref. 2). Bottom panel:  $\kappa=12$  cm<sup>-1</sup> corrected for experimental pulse spectrum and *ad hoc* population relaxation (see text). Each spectrum is normalized to its maximum.

parison, we corrected the simulated spectra for the experimental excitation pulse spectrum. Population relaxation effects are now included by applying an *ad hoc* relaxation factor using a population life time  $T_1=200$  fs.<sup>1</sup> Additionally, we included a persisting ground state bleach to match the experimental conditions. For multimode nonadiabatic simulations, a strict separation of the different contributions to the nonlinear signal is not possible. We approximated the persisting ground state bleach by only considering diagonal contributions to the respective nonlinear response function  $S_1$  and  $S_4$ .<sup>12</sup> With these assumptions, our simulations are in close agreement with the experiment for peaks shapes, amplitudes, and dynamics.

Our new simulation procedure provides the first nonlinear response treatment of highly disordered vibrational excitons, which explicitly allows multiple state crossing between vibrational energy surfaces. With no separation of time scales between the transfer and fluctuation processes, the nonadiabatic nature of the transfer process is thus fully accounted for. The explicit treatment of these processes, as well as intra- and intermolecular vibrational anharmonicities, and the fluctuations and anharmonicities of the transition dipole moments facilitated in the NISE approach provides the highest level description of the nonlinear vibrational response of water to date.

Many interesting features of the PP and 2DIR-PE response are caused by the mixing between states in the 2D anharmonic OH stretch potential. This is markedly different from the two decoupled one-dimensional stretch potentials in HOD. The fundamental transitions show an increased sensitivity to bath fluctuations, mainly caused by resonantly enhanced fluctuations in orientation and amplitudes of the transition dipole moments, i.e., non-Condon effects.<sup>5</sup> The fluctuations in the local basis result in changes in the character and symmetry of the modes, and can, therefore, to some degree be interpreted as intramolecular ET. Mixing of

the overtone states further leads to strong intramolecular anharmonicities. In particular, the harmonic selection rules are lifted, opening up additional pathways contributing to the nonlinear response. These effects manifest the increased sensitivity of the OH stretch vibrations to fluctuations in the hydrogen bond network in water, compared to isotopically substituted systems such as HOD/D<sub>2</sub>O or HOD/H<sub>2</sub>O.<sup>3,4</sup> In our results, this is evident in the fast loss of correlation in the 2DIR-PE spectra (Fig. 3) and the fast decay of PA transients (Fig. 2) even for the uncoupled system.

The main result of the intermolecular coupling is observed in the PA (see Fig. 2). The experiment is reproduced for  $\kappa=12$  cm<sup>-1</sup> which can be considered to be surprisingly small. Previous theoretical<sup>8,9</sup> work had to invoke much larger couplings to reproduce the extremely fast time scales of the PA decay in H<sub>2</sub>O. Here, we show that the large number of acceptor modes, as well as anharmonicities and fluctuations in the system open up many intermolecular transfer pathways, which lead to a full decay of the PA on time scales observed in the experiment<sup>1,2,16</sup> even for these small average couplings. The effect of the ET on the 2DIR-PE spectra is found to be rather small (see Fig. 3). Only for large  $t_2$  (>200 fs), somewhat faster dynamics in the coupled system become apparent. We conclude that most of the fast dynamics in the 2DIR-PE spectrum of H<sub>2</sub>O are indeed caused by the increased sensitivity of the OH stretch potential to anharmonic bath coupling. Consequently, the OH stretch vibration is shown to be an excellent probe of the hydrogen bond network in H<sub>2</sub>O.

In summary, we presented simulations of the 2DIR-PE and PP response of the OH stretch vibration in liquid water. Our new technique using numerical integration of the Schrödinger equation allowed explicit treatment of intermolecular vibrational couplings and nonadiabatic effects for the first time. The 2D OH stretch potential was shown to be

extremely sensitive to bath fluctuations resulting in very fast spectral diffusion dynamics. We also found surprisingly small intermolecular couplings to be fully sufficient to reproduce experimentally observed energy transfer times. The simulation results are in close agreement with our most recent experimental work.<sup>2</sup>

## ACKNOWLEDGMENTS

This research was supported by the Canadian Institute of Photonics Innovation, Photonics Research Ontario, and the Natural Sciences and Engineering Research Council of Canada. S.M. gratefully acknowledges the support of NIH (Grant No. GM59230) and NSF (Grant No. CHE-0745892). A.P. thanks Thomas la Cour Jansen for helpful discussions.

<sup>1</sup>M. L. Cowan, B. D. Bruner, N. Huse, J. R. Dwyer, B. Chugh, E. T. J. Nibbering, T. Elsaesser, and R. J. D. Miller, *Nature (London)* **434**, 199 (2005).

<sup>2</sup>D. Kraemer, M. L. Cowan, A. Paarmann, N. Huse, E. T. J. Nibbering, T. Elsaesser, and R. J. Dwayne Miller, *Proc. Natl. Acad. Sci. U.S.A.* **105**,

437 (2008).

<sup>3</sup>C. J. Fecko, J. D. Eaves, J. J. Loparo, A. Tokmakoff, and P. L. Geissler, *Science* **301**, 1698 (2003).

<sup>4</sup>J. B. Asbury, T. Steinel, K. Kwak, C. P. Lawrence, J. L. Skinner, and M. D. J. Fayer, *J. Chem. Phys.* **121**, 12431 (2004).

<sup>5</sup>J. R. Schmidt, S. A. Corcelli, and J. L. Skinner, *J. Chem. Phys.* **123**, 044513 (2005).

<sup>6</sup>T. Hayashi, T. I. C. Jansen, W. Zhuang, and S. Mukamel, *J. Phys. Chem. A* **109**, 64 (2005).

<sup>7</sup>R. DeVane, B. Space, A. Perry, C. Neipert, and C. Ridley, and T. Keyes, *J. Chem. Phys.* **121**, 3688 (2004).

<sup>8</sup>H. Torii, *J. Phys. Chem. A* **110**, 8422 (2006).

<sup>9</sup>J. A. Poulsen, G. Nyman, and S. Nordholm, *J. Phys. Chem. A* **107**, 8420 (2003).

<sup>10</sup>T. I. C. Jansen and J. Knoester, *J. Phys. Chem. B* **110**, 22910 (2006).

<sup>11</sup>H. J. C. Berendsen, D. van der Spoel, and R. van Drunen, *Comput. Phys. Commun.* **91**, 43 (1995).

<sup>12</sup>A. Paarmann, T. Hayashi, S. Mukamel, and R. J. D. Miller (unpublished).

<sup>13</sup>S. Ashihara, N. Huse, A. Espagne, E. T. J. Nibbering, and T. Elsaesser, *J. Phys. Chem. A* **111**, 743 (2007).

<sup>14</sup>S. Mukamel, *Principles of Nonlinear Optical Spectroscopy* (Oxford University Press, New York, 1995).

<sup>15</sup>R. Kosloff, *J. Phys. Chem.* **92**, 2087 (1988).

<sup>16</sup>S. Woutersen and H. Bakker, *Nature (London)* **402**, 507 (1999).